Cent. Eur. J. Geosci. • 3(1) • 2011 • 77-89
DOI: 10.2478/s13533-011-0011-9

Springer

Central European Journal of **Geosciences**

State of stress in the northern Tabas block, east-central Iran, as inferred from focal mechanisms of the 1978 Tabas earthquake sequence.

Research Article

Behzad Zamani G.*

Department of Geology, Faculty of Natural Sciences, University of Tabriz, Tabriz, Iran

Received 21 November 2010; accepted 28 February 2011

Abstract: In this paper, the state of stress in the northern Tabas block in east-central Iran is analyzed based on the systematic inversion of aftershock focal mechanisms from the 1978.09.16 Tabas earthquake, to characterise the stress regime that controls most earthquakes in this area. Here, stress inversions of double-couple focal mechanisms of earthquakes recorded during the 30 days following the main shock have been carried out. The calculated average stress regime indicates dominant major 226° to 237° trending compression for the Tabas region. The dominating regime in east-central Iran is thrusting with a minimum stress axis, σ_3, close to vertical. The reconstruction of the main seismotectonic stress in east-central Iran with a NE-SW compression is consistent with independent information of the active plate convergence related to Arabia-Eurasia convergence. Most earthquakes in the mentioned area occur near or around concealed Quaternary thrust faults with their activity being controlled by the NE-SW compression. Where Φ, the ratio of principal stress differences, is 0.5, a small difference between σ_2, σ_3 and σ_1 and small amounts of deviatoric stress is indicated. Therefore, for small deviatoric horizontal σ_1 it is not possible to increase and reactivate small sections of basement thrust faults and create secondary basement aftershocks. Reconstructed stress regimes in this study for sedimentary cover (237) and basement (226) of Tabas are similar. Therefore, it seems that the basement and cover were coupled together, possibly along the 2-4 km of upper Precambrian low-grade metamorphic rocks. Then these segments of the fold-and-thrust belt were involved in similar seismic activity under a similar stress regime.

Keywords: State of stress • east-central Iran • focal mechanisms • inversion

1. Introduction

Iran is located within the convergence domain between the Arabian and Eurasian plates. The central parts of Iran move northwards with respect to western Afghanistan at ~15 mm yr^{-1} [1]. This northward motion introduces ~15 mm yr^{-1} of north-south right-lateral shear across eastern Iran which is accommodated on right-lateral strike-slip fault systems on both the western (Gowak-Nayband fault system) and eastern (Neh and Zendan fault systems) margins of the aseismic Dashte-e Lut desert [2, 3]. The study area is situated in the eastern part of central Iran, and northern part of the Tabas block

*E-mail: b.zamani@tabrizu.ac.ir, Tel: +98 411 3392700, fax: +98 411 4448914

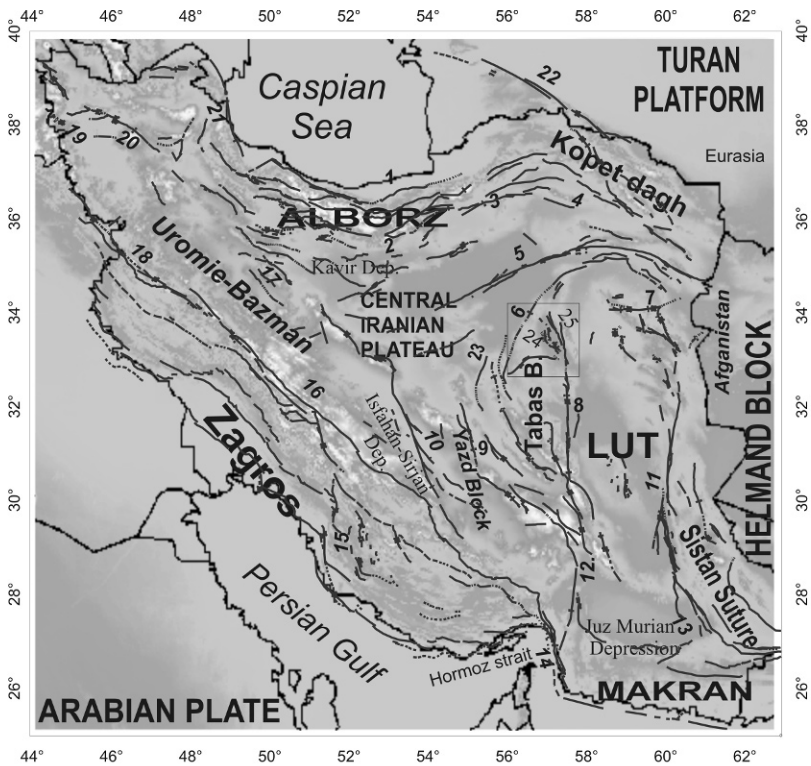

Figure 1. Tectonic setting of Iran. Study area is marked as grey rectangle and major fault zones adapted from [4] are numbered as follows: 1: Khazar Fault, 2: Alborz fault, 3: Trod fault, 4: Miami fault, 5: Dourone Fault, 6: Kalmard Fault, 7: Dasht-e-Bayaz Fault, 8: Naiband Fault, 9: Anar Fault, 10: Dehshir Baft Fault, 11: Bakhtar-Neh Fault, 12: Neh and Zendan fault, 13: Bashagard Fault, 14: Minab Fault, 15: Kazeron Fault, 16: Main Zagros Reverse Fault , 17: Gom Zafre Fault, 18: Main Recent Fault, 19: Uromie Fault, 20: North Tabriz Fault, 21: Astara Fault, 22: Eshg Abad Fault, 23: Poshte Badam Block, 24: Tabas fault, 25: Shotori mountain Range. Simplified pattern of major lithospheric blocks in Iran are adapted from [4] and [38] block names indicated in black.

(Fig. 1). Tabas is a town with approximately 30,000 inhabitants, 950 kilometers southeast of Tehran. The city was hit by a major destructive earthquake on September 16th 1978, during which about 22,000 lost their lives. The recorded earthquake magnitude was between 7.5 and 7.9 on the Richter scale. Despite the major tectonic hazard in the Tabas region, relatively few studies have attempted to analyze the local-scale seismotectonic stress regime. Consequently, this research aims to characterise the stress regime which controls most of the earthquakes occurring in this area through an inversion of the earthquake focal mechanisms.

2. Geodynamic setting

Iran is a typical example of a Late Cenozoic continent-continent collision zone in the middle of the Alpine-Himalayan belt. The tectonics of the Iranian region is governed by the convergence between the Arabian and Eurasian plates [5, 6]. In the Hormoz Strait region of southern Iran, the direction of convergence between Arabia and Eurasia is N-S to NNE-SSW.

The closure of the Neo-Tethys oceanic domains occurred in the Mesozoic and Early Cenozoic times and was followed by continental shortening during the Late Cenozoic after the major collision of the Zagros. Between the northern (Alborz) and southern (Zagros) mountain belts, the lithosphere of the Iranian plateau was formed by the accretion of successively folded zones resulting from earlier orogenies following the closure of the ancient Tethyan ocean basin. The historical [7] and instrumental seismicity [8] in Iran suggest intra-continental deformation concentrated in several mountain belts surrounding relatively major, but mostly aseismic blocks of central Iran, Lut and South Caspian [9].

In eastern Iran, right-lateral shear is accommodated along several large N-S trending, right-lateral fault systems. In the north, right-lateral shear is inferred from clockwise rotation of east-west left-lateral faults (the Doruneh and Dasht-e-Bayaz faults).

In the north of the study area, Doruneh fault is one of the longest and most clearly identifiable active faults in Iran, accommodating right-lateral shear between central Iran and Afghanistan [9]. Relatively few earthquakes have been recorded on this fault despite the clear expression of morphotectonic and seismic activity [10]. The low rate of seismic activity and the few earthquakes on the Doruneh fault is in contrast to the neighboring Dasht-e-Bayaz region in the west of the study area, which appears to play an important role in the regional tectonics (e.g. [11]). Shortening components associated with the strike-slip faults result in widespread thrust faulting. These thrust faults often fail to reach the surface (blind or 'concealed' faults).

Central Iran, including the study area, is a mosaic of various tectonic blocks once separated by minor basins [12] that started to close in the mid-Tertiary [13] because of plate convergence. However, much of the border collision zone did not start to deform until the Mid-Miocene or later [14]. Alavi [15], recognizing long strike-slip dextral faults (Nayband, Kalmard, Kuhbanan, and Posht-e-Badam), divided central Iran into four major sub-blocks: Lut, Posht-e-Badam, Yazd and Tabas (Fig. 1). The area considered here is situated within the northern Tabas block, east of central Iran.

Tabas area was considered the western part of the "rigid" Lut block and was named "Tabas block". The city of Tabas is at the foot of the Shotori fold and thrust mountain belt. This mountain belt is composed of a sedimentary rock sequence (1500 m) of Paleozoic to Tertiary age [16, 17]. In the Paleozoic-Mesozoic, this region was a sedimentary basin which underwent continuous rifting before the late Tertiary when a compressional phase caused uplift [18].

3. Seismotectonic activity

Compared to the high rate of deformation and intense seismic activity observed in the Zagros mountain ranges in southern Iran and Alborz and Kopet-Dagh (Fig. 1) mountain ranges [19] in northern Iran, east-central Iran is generally considered to be relatively quiet seismically [5]. During recent years, however, there has been an increase in large and moderate earthquake activity in central Iran. The most significant earthquakes include the June 10^{th}, 1939 Baharestan earthquake (m_b=5.5), the August 31^{st}, 1968 Dasht-e- Bayaz earthquake (M_s=7.3), the September 1^{st}, 1968 Ferdows earthquake (M_s= 6.4), the May 5^{th}, 1973 Shahzadeh earthquake (m_b=5.1), the June 17^{th}, 1974 Posha earthquake (m_b= 4.8), the September 16^{th}, 1978 Tabas earthquake (M_s= 7.7), and the November 27^{th} 1979 Qainat earthquake (M_s= 7.1).

The Tabas earthquake occurred 170 km west-southwest of the destructive 1968 Dasht-e-Bayaz earthquake. The main shock occurred in the evening at 19:38:18 local time (15:35:56.6 UTC) without any perceptible foreshocks [20]. The main shock was followed by several aftershocks. Ten days after the main shock, the Geological Survey of Iran and a team from the University of Cambridge set up an array of nine portable seismometers which operated for 30 days to record aftershocks.

The Tabas fault is one of the principal late Precambrian faults in the western part of the Shotori basin, reactivated as a normal and thrust fault during different tensional and compressional phases [21]. Surface rupture on this fault occurred mainly along a major reverse late Quaternary fault (Tabas fault) that is not a single continuous fault, rather it is composed of a several segments. It extends for about 85 km in ten segments in a curved NNW-SSE direction [21] and thrusts the Neogene sediments and Shotori range in the east over the Tabas compressional depression in the west. Tabas fault segments are separated by gaps in the surface rupture and are composed of several parallel thrust faults developed in a zone about 30 m wide.

Some reverse and transverse faults in the Shotori Range, east of Tabas, were active during the late Quaternary and cut recent alluvial fans and river terraces.

Tabas is the eastern part of the central Iranian seismotectonic province which is composed of several horsts and grabens [20]. Central Iran has scattered seismic activity with long recurrence periods of large magnitude earthquakes, and seismic gaps along several recent Quaternary faults [18] where the earthquakes are generally shallow [22].

Determining earthquake hypocentral locations and focal mechanisms play a major role in the understanding of active tectonic processes. The following sections will be focussing on the significance of earthquake focal mechanisms in terms of regional seismotectonic stress.

4. Data

The data from aftershock focal mechanisms listed in Berberian [18] catalogue (see detailed explanation in [20]) were used as input data for stress inversion. These earthquakes were recorded by an array of nine portable seismometers deployed for 30 days following the main shock of 16^{th} September, 1978 Tabas earthquake, by the Geological Survey of Iran and the University of Cambridge.

In order to improve the accuracy of the routinely determined hypocenters, epicentres and origin times, Berberian [18] adopted two techniques: relative hypocentral location (23, 24) and waveform modelling [25] (also adopted in this study). Berberian [18] used a group of well-recorded earthquakes fixed at a certain depth, and used the location program *Hypo-75* to calculate the optimum parameters. He plots root mean square (RMS) residuals versus the fixed depths, with S-readings that were located using different fixed depths and a single layer model, which shows that the model and seismometer network had a good depth resolution.

In this study, events recorded at less than 5 stations or with standard errors greater than 2 km in depth or epicentre were disregarded. In addition, because aftershocks with shallow focal depths (<4 km) usually have large depth errors, these too were disregarded. Therefore, the study is based entirely on those events with high quality locations. The body-wave magnitude of the events is in the range 1.5-3.79.

Berberian [18] proposed that the Tabas-Shotori region is possibly underlain by three rheological zones. First, a low-strength top zone (0-3 Km), second, an intermediate seismic zone (3-23 Km) and third, a lower ductile zone (below 23 Km). However, he divided the focal mechanisms of earthquakes into two parts (sedimentary cover and basement events) using the strike of nodal planes and the event depths. Thirty-five earthquakes occurred in the sedimentary cover (<12 km depth) and 25 in the basement (>12 km depth). An epicentre map of these earthquakes is shown in Figs. 2 and 3 for the sedimentary cover and basement aftershocks respectively. For more details about the original data, the reader is referred to the source paper [18, 20].

5. Results of seismotectonic stress inversion

The method of Angelier [26] is adopted in this research to obtain the stress state that best accounts for a set of double-couple earthquake focal mechanisms. The method is based on the slip shear stress component (SSSC) criterion. The SSSC is the component of stress acting in the slip direction of a fault. The stress tensor is reduced to four unknowns, since sole consideration of shear stress orientations cannot give access to the isotropic component and scale factor of stress [27]. The sum of the SSSC values is maximized as a function of four unknowns that describe the reduced stress tensor, including the orientations of the principal stress axes (σ_1, maximum compressive stress; σ_2, intermediate stress and σ_3, minimum stress) and the ratio between the principal stress differences $\Phi = [\sigma_2\text{-}\sigma_3]/[\sigma_1\text{-}\sigma_3]$. In this method no choice between the nodal planes is needed prior to or during the inversion. The run time is negligible considering the size of the data set, because the inversion is carried out by analytical means. This facilitates inclusion of the inversion in a variety of processes for separating or refining the data. Such properties were important in this study for refining the data. Therefore the advantages of this method are, first, there is no need to choose between the nodal planes of each focal mechanism due to the intrinsic properties of the SSSC; second, the runtime is negligible, because the inverse problem is solved using analytical means so that the numerical aspects are reduced to a minimum.

INVGLI is the stress analysis software used in this study, written by Professor Angelier.

The results of stress inversion in the Tabas region are summarised in Figures 2, 3 and 4, and Table 1. In Figure 2 & 3 pairs of arrows indicate compression trends resulting from the application of the direct inversion for sedimentary cover aftershock and basement aftershock events respectively. In Table 1, some major parameters of the direct inversion have been added. In particular, ω_{acc} is the threshold value adopted after application of a specific refining process (see detailed explanation in [26]).

This value corresponds to the variable bound chosen for the inversion criterion ω (ranging from -100% for total misfit to 100% for perfect fit). As a consequence of the moderate fit demand of 5%, the number of accepted earthquake focal mechanisms, N_{acc}, is large with respect to the number of considered focal mechanisms. The other numerical results include the trends and plunges of the stress axes σ_1, σ_2 and σ_3 and the ratio Φ.

6. Discussion and conclusion

The stress inversion allows determination of a consistent average state of stress in the east-central Iran region, based on available focal mechanisms for the aftershock sequence of the 1978 Tabas earthquake. This average stress is characterised by a NE-SW (226°) compression (maximum compressive stress σ_1), the minimum stress axis being close to vertical for the basement of the Tabas region (>12 km). The calculated stress regime thus indicates a dominant thrusting mode for the basement. The dominating reverse-type stress is consistent with the evidence of reverse faults and focal mechanisms in this region. Because the value of the parameter Φ is equal 0.5, this stress regime does not contradict the presence of active strike-slip faults and focal mechanisms of earthquakes. This result is consistent with Walker et al. [30]. Accordingly, body-wave seismograms for two earthquakes in September 1968 near Ferdows (150 km east of Tabas) indicated thrust faulting at depths of about 10 km. The activity of concealed Quaternary thrust faults is also controlled by the NE-SW compression in east-central Iran.

In the sedimentary cover of Tabas region, the average

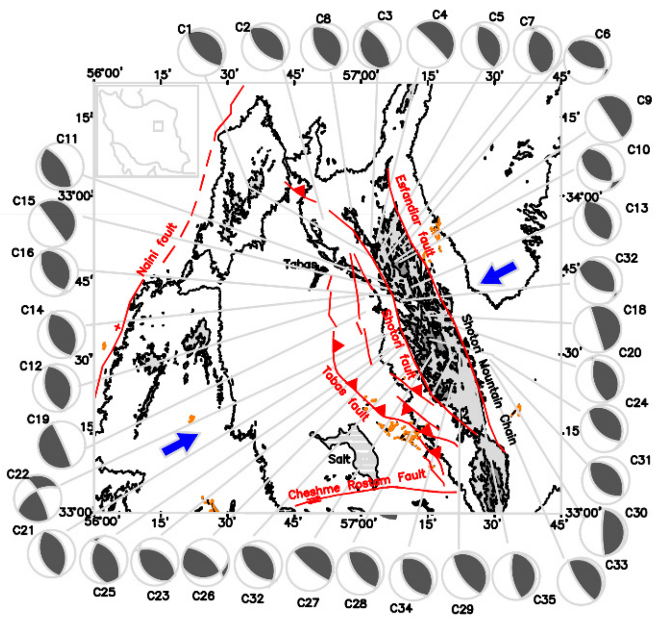

Figure 2. Focal mechanisms of earthquakes for sedimentary cover aftershock events, in east central Iran. Small stereoplots are 'beachball' illustrations of double-couple focal mechanisms (Schmidt's projection, lower hemisphere, tension and pressure dihedra plotted as black and white respectively). The study area is shown as a rectangle in the inset map. Major fault zones shown as thick lines adapted from [4] and [18]. Results of the direct inversion method to determine average stress tensors, stress axes σ_1 (maximum compressive principal stress) as pair of arrows indicate corresponding trends of compression. Numerical parameters given in Table 1. Reference numbers of focal mechanisms are as in [18].

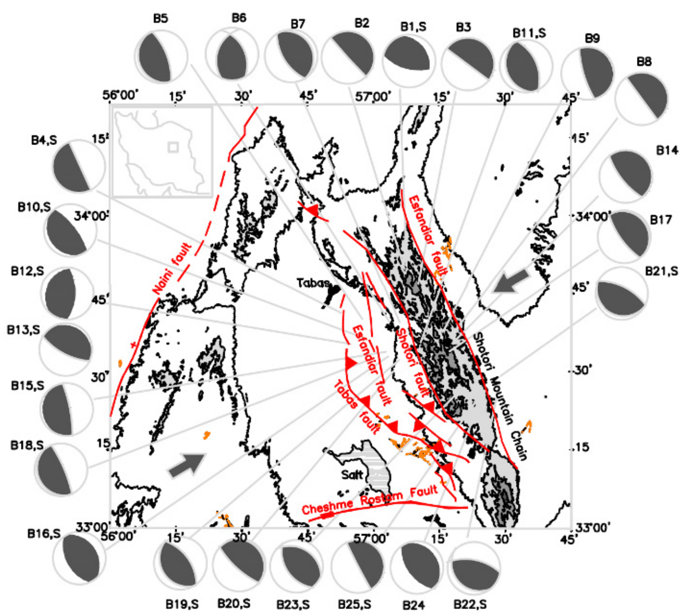

Figure 3. Focal mechanisms of earthquakes for basement aftershock events, in east-central Iran. Numerical parameters given in Table 1. All labels as in Fig. 2. Reference numbers of focal mechanisms are as in [18].

Table 1. Numerical results of the direct inversion to determine stress tensors, for east-central Iran, northern Tabas. ω_{acc}, threshold value adopted after application of refining process for the inversion criterion ω (ranging from -100% for total misfit to 100% for perfect fit). In agreement with average estimated uncertainties in earthquake focal mechanisms, the stage with a 5.0% threshold value of ω has been adopted, except when identical rejection rate provides a better value, 4.5% or 5.0%. N_{acc}, number of accepted earthquake focal mechanisms in percent. Stress axes σ_1, σ_2 and σ_3 (maximum compressive, intermediate and minimum principal stress, respectively) with orientation given as trend and plunge in degrees. Φ, ratio of principal stress differences Φ=(σ_2-σ_3)/(σ_1-σ_3) as defined by [28] and [29]. ω_m and ω_{sd}, average a posteriori estimator ω (from -100%, total misfit, to 100%, perfect fit) and standard deviation, as percentages. Auxiliary estimators: τ^*_m and τ^*_{sd} for the average shear stress as percentage of maximum shear stress (0% to 100%) and its standard deviation, in percentages α_m and α_{sd} for the average angle between observed slip and calculated shear stress, in degrees. Detailed explanation of the method in [26].

Reg.	ω_{acc}	$N_{acc\%}$	σ_1		σ_2		σ_3		Φ	$\omega_{m\%}$	ω_{sd}	$\tau_{m\%}$	τ_{sd}	α_m	α_{sd}
Sedimentary Cover	5	87	237	18	147	0	56	72	0.52	81	15	83	15	11	8
Basement	5	59	226	33	136	0	46	57	0.5	91	6	93	6	9	8

stress is characterised by a NE-SW (237°) compression (maximum compressive stress σ_1), the minimum stress axis being close to vertical. The calculated stress regime thus indicates a dominating thrusting mode for sedimentary cover. This stress regime does not contradict the presence of strike-slip active faults and focal mechanisms of earthquakes.

The NE-SW compression (trend 226° to 237°) reconstructed herein is consistent with the convergence direction suggested by recent geodetic GPS studies [4, 31, 32]. Note that the present determination of seismotectonic compressive stress and the kinematic determinations in the same region are fully independent.

These results are also compatible with the earlier kinematic results from [33] and [5] regarding the convergence across Iran, between Eurasia and Africa-Arabia.

Geodetic methods can be used to measure the strain in the upper crust. The calculation of strain directions may depend on magnitude and the fault system activity during the sampling period. If two fault populations exist, then estimates of the strain orientation may vary as a function of time, depending on which fault system is active. Thus, the estimate of strain directions is not meaningless but may depend rather strongly on time and magnitude. Therefore, some differences between this study and geodetic results could be due to the time and magnitude dependence of strain.

Sarkar et al., [34] have analysed sub-events of the Tabas earthquake and claimed that the fault plane solutions of earthquakes generally show WNW–ESE strikes, subparallel to the regional strike of the documented main fault systems. In addition, they concluded that the preferred fault planes correspond to the main event and to the following sub-events strike of ESE–WNW and steep dip angles, and exhibit predominantly reverse thrust motion with some left-lateral strike-slip components. Such a slip process is in agreement with a northwesterly propagating rupture initiated at the base of a listric thrust fault. These interpretations are consistent with the compressive stress orientation (237° and 226°) resulting from this study, nearly perpendicular to the WNW-ESE average strike of the fault system (the Tabas thrust fault and other concealed thrust faults) and the Shotori mountain range (Fig. 1).

Berberian, [18] studied the aftershocks of the 1978 Tabas earthquake sequence and found that almost all these aftershocks followed the pattern of faulting at the surface and occurred in the hanging-wall of active faults. The hypocentres of these aftershocks mainly occurred at depths shallower than 23 km, with a high concentration of seismic activity between 8 and 14 km depths. He suggested that the focal mechanisms of the aftershock sequences are consistent with an overall NNE continental shortening in Iran. Also, his calculated P-axes for the solutions showed an average trend of 045 and plunged slightly toward NE for both sedimentary cover and basement mechanisms. Therefore, reconstructed stress regimes are consistent with Berberian's [18] interpretation.

By analyzing the stress (using the method of Gephart and Forsyth, [36]) and by comparison of strain and stress tensor orientations for parts of Iran, Gillard and Wyss [35] concluded that the stress orientations are mainly similar along all Iranian plate boundaries. In this study the greatest principal stress in east-central Iran (northern Tabas) is horizontal and oriented NE-SW (18/237 and 33/226) which is consistent with the results of Gillard and Wyss [35] in Eastern Iran (02/061).

Berberian [37] suggested that the significant difference between shallow and deep aftershocks mechanisms may indicate that after sudden release of stress during the main-shock, the value of regional shearing stress in the basement would increase locally to values sufficiently high to reactivate small sections of the basement thrust faults and cause the secondary basement aftershocks. Stress analysis results in this study are characterised by NE-SW compression (maximum compressive stress σ_1) with the maximum stress axis being close to horizontal for the basement in the Tabas region (>12 km). The value of

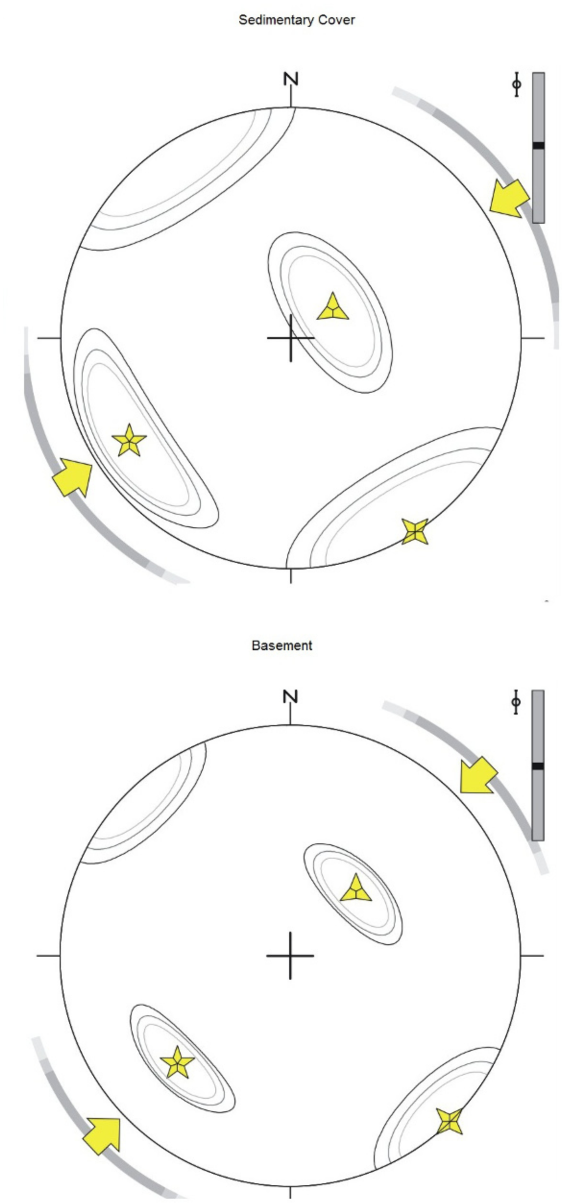

Figure 4. Graphic results of the direct inversion to determine average stress tensors according to Angelier's method (2002), analysed separately for Sedimentary Cover (upper plot) and Basement (lower plot) in the northern Tabas block. Stereoplots with equal-area projection of lower hemisphere. Numerical parameters given in Table 1. Stress axes $\sigma 1$, $\sigma 2$ and $\sigma 3$ (maximum compressive, intermediate and minimum principal stress, respectively) as 5, 4 and 3-pointed stars respectively, with 60, 75 and 90% confidence ellipses plotted. Pairs of arrows indicate corresponding trends of compression and extension, with azimuth uncertainties in grey levels. Φ value and its uncertainties added as a scale bar (from 0 to 1) in upper-right corner of each stereoplot.

Φ (0.5, Table 1) indicates small differences between σ_2, $\sigma_3$and σ_1, and small amount of deviatoric stress. Therefore inconsistent with Berberian [20, 37], for small deviatoric horizontal σ_1 it is apparently not possible to increase and reactivate small sections of the basement thrust faults and create the secondary basement aftershocks.

Reconstructed stress regimes in this study for sedimentary cover (237) and basement (226) of Tabas are similar. Therefore it seems the basement and cover were coupled, possibly along the 2-4 km of upper Precambrian low grade metamorphic (thick-skin tectonic model), and then segments of this fold-thrust belt were involved in similar seismic activity and stress regime.

Acknowledgements

The Tabriz University and the Ministry of the Sciences, Research and Technology of Iran supported the work. I dedicate this research to Prof. Jacques Angelier (deceased). In addition, I gratefully thank Mr. Behnam Zamani, for his detailed grammatical review. Special thanks are due to anonymous reviewers for their helpful and detailed reviews.

References

[1] Vernant Ph., Nilforoushan F., Hatzfeld D., Abbasi M.R., Vigny C., Masson F., Nank-ali H., Martinod J., et al., Present-day crustal deformation and plate kinematics in the Middle East constrained by GPS measurements in Iran and northern Oman. Geophys. J. Int., 2004,157, 381-398

[2] Walker R., J. Jackson, Active tectonics and late Cenozoic strain distribution in central and eastern Iran. Tectonics, 2004, 23, TC5010, doi:10.1029/2003TC001529.v

[3] Regard V., O.Bellier J.-C., Thomas D., Bourl'es S., Bonnet M. R., Abbassi R., Braucher J., Mercier E., et al., Cumulative right-lateral fault slip rate across the Zagros–Makran, transfer zone: role of the Minab–Zendan fault system in accommodating Arabia–Eurasia convergence in southeast Iran. Geophys. J. Int., 2005,162,177–203

[4] Hessami K., Jamali F., Tabasi H., Major Active Faults map of Iran, Scale 1:2500000, 2003. International Institute of Earthquake Engineering and Seismology (IIEES), 1 sheet

[5] Jackson J.A., McKenzie D.P., Active tectonics of the Alpine-Himalayan belt between western Turkey and Pakistan, Geophys. J. R. Astr. Soc., 1984. 77, 185-264

[6] Jackson J.A., McKenzie D., The relationship between plate motions and seismic moment tensors, and the

rates of active deformation in the Mediterranean and Middle East. Geophys. J. Int., 1988, 95, 45-73

[7] Ambraseys N., Melville C., A History of Persian Earthquakes. Cambridge University Press, Cambridge, UK, 1982

[8] Engdahl E. R., Van der Hilst R., Buland R., Global teleseismic earthquake relocation with improved travel times and procedures for depth determination. B. Seismol. Soc. Am., 1998, 88, 722-743

[9] Fattahi M., Walker R.T., Khatib M. M., Dolati A., and Bahroudi A., Slip-rate estimate and past earthquakes on the Doruneh fault, eastern Iran. Geophys. J. Int., 2007,168, 691-709

[10] Ambraseys N., Melville C., The seismicity of Kuhistan, Iran. Geogr. J., 1977, 143, 179–199

[11] Walker R., Jackson J., Active tectonics and Late Cenozoic strain distribution in central and eastern Iran. Tectonics, 2004, 23, TC5010, doi:10.1029/2003TC001529

[12] Berberian M., King G.C.P., Towards a paleogeography and tectonic evolution of Iran. *Can. J. Earth Sci.*, 1981. 18, 210–285

[13] McCall G.J.H., The inner Mesozoic to Eocene ocean of south and central Iran and associated microcontinents. Geotectonics, 1996. 29, 490-499

[14] Dewey J.F., Hempton M.R., Kidd W.S.F., Saroglu F., Sengor A.M.C., Shortening of continental lithosphere; the neotectonics of eastern Anatolia, a young collision zone. Special Publication of the Geological Society London, 1986, 19, 3-36

[15] Alavi M., Tectonic map of the Middle East. Geological Survey of Iran, 1991, 1 sheet

[16] Stocklin J., Eftekharnejad-Nezhad J., Hushmandzadeh A., Geology of Shotori Range (Tabas area, East Iran). Geological Survey of Iran, Report no 3, 1965

[17] Ruttner A., Nabavi M. H., Hajian J., Geology of the Shirgasht area (Tabas, East Iran). Geological Survey of Iran, Report no 4, 1968

[18] Berbarian M., Aftershock tectonics of the 1978 Tabas-e-Golshan (Iran) earthquake' sequence: a documented active 'thin and thick-skinned tectonic' case. Geophys. J. R. Astr. Soc., 1982, 68, 499–530

[19] Zamani B.G., Angelier J., Zamani A., State of stress induced by plate convergence and stress partitioning in northeastern Iran, as indicated by focal mechanisms of earthquakes. J. Geodyn., 2008, 45, 123-130

[20] Berberian M., Continental deformation in the Iranian Plateau, "Contribution to the Seismotectonics of Iran, Part IV", Geological Survey of Iran, Tehran, Rep. 1983, No. 52, PP.415, 444

[21] Berberian M., Tabas-e-Golshan (Iran) catastrophic earthquake of 16 September 1978; a preliminary field report. Disaster, 1979, 2, 207-219

[22] Berberian M., "Contribution to the Seismotectonics of Iran Part 10", Geological Survey of Iran, Tehran, Rep. 1976, No. 39, 518 P

[23] Fitch T.J., Compressional velocity in source regions of deep earthquakes: an application of the master event technique, Earth and planetary science Letters ,1975, 26, 156-166

[24] Jackson J.A., Fitch T.J., Seismotectonic implications of relocated aftershock sequences in Iran and Turkey. Geophys. J. R. Astr. Soc., 1979, 57, 209-229

[25] Helmberger D.V., Burdick L. J., Synthetic Seismograms. Ann. Rev. Earth Planet. Sci. Lett., 1979, 7, 417-442

[26] Angelier J., Inversion of earthquake focal mechanisms to obtain the seismotectonic stress (a new method free of choice among nodal planes) IV, Geophys. J. Int., 2002, 150, 588-609

[27] Angelier J., Tectonic analyses of fault slip data sets. J. Geophys. Res., 1984, 89, 5835-5848

[28] Angelier J., Sur l'analyase de measures recueillies des sites failles: l'utillite d'une confrontation entre les methods dynamiques et cinematiques. (On measure of analysis sites collected faults: Utilities of confrontation between dynamic and kinematics methods), C. R. Hebd. Seanc. Acad. Sci., 1975, 281, 1805-1808

[29] Angelier J., From orientation to magnitudes in paleostress determinations using fault slip data. J. Struct. Geol., 1989, 1/2, 37-50

[30] Walker R., Jackson J., Baker C., Surface expression of thrust faulting in eastern Iran: source parameters and surface deformation of the 1978 Tabas and 1968 Ferdows earthquake sequences. Geophys. J. Int., 152, 2003,749-765

[31] Nilforoushan F., Masson F., Vernant P., Vigny C., Martinod J., Abbasi M., Nankali H., Hatzfeld D., et al., GPS network monitors the Arabia-Eurasia Collision deformation in Iran. Journal of Geodesy, 2003, 77, 411-422

[32] Masson F., Anvari M., Djamour Y., Walpersdorf A., Tavakoli F., Daignieres M., Nankali H., Van Gorp S., Large-scale velocity field and strain tensor in Iran inferred from GPS measurements: new insight for the present-day deformation pattern within NE Iran. Earth Planet. Sc. Lett., 2006, 252, 180-188

[33] McKenzie D., Active tectonics of the Mediterranean region. Geophy. J. R. Astr. Soc., 1972. 30, 109-185.

[34] Sarkar I., SriRam V., Hamzehloo H., Khattri K.N., 2005, Subevent analysis for the Tabas earthquake of September 16, using near field accelerograms. Physics Earth and Planetary Interiors, 1978, 151,

53-76

[35] Gillard D., Wyss M., Comparison of strain and Stress tensor orientation: Application to Iran and Southern California. J. Geophys. Res., 1995, 100, 197-213

[36] Gephart J.W., Forsyth D.W., An improved method for determining the regional stress tensor using earthquake focal mechanism data: Application to the San Fernando earthquake sequence. J. Geophys. Res., 1948, 89, 9305-9320

[37] King G., Soufleris C., Berberian M., The source parameters, surface deformation and Tectonic setting of three recent earthquakes, Thessalonki Greece. 1981, Disasters, (5)1, 36-46. Wiley-Blackwell pub.

[38] Zamani B., Study of Tectonic Stress State of Iran, Ph.D. thesis, Shiraz University, Iran, 2009

Appendix

Data analyzed for reconstruction of stress state. The single data lines indicated a fault solution for a single event, but for composite solutions the average location of the group are indicated by the entry with no time and date. The magnitudes of the used events were between 1.5 to 2 in 15 events and 2 to 3.79 for aftershocks.

No. is the number of each mechanism. Date (yyyymmdd) and time (hhmmss) follow usual convention and all angles are in degrees. Lat.(N) is latitude and Long.(E) is longitude of the earthquake hypocentres. Depth is the focal depth of the earthquakes in km.

For each focal mechanism, the two nodal planes (NP1 and NP2) are characterised by the strike (Str), the dip (Dp). The rake of the inferred motion vector (S1 and S2) are characterised by the strike (Str) and the dip (Dp).

Basement

No.	yyyy	mm	dd	hh	Mm	ss	Lat.(N)	Long.(E)	Depth	NP1		S1		NP2		S2	
									(Km)	Str	Dp	Dp	Str	Str	Dp	Dp	Str
1	1978	10	18	2	9	15	33.75	59.97	9.3	152	30	30	62	332	60	60	242
2	1978	10	20	4	52	38	33.72	56.88	10.68	139	28	28	43	313	62	61	230
3							33.67	57.03	9.59	146	70	77	56	354	19	18	254
	1978	10	7	18	41	36	33.65	57.07	8.72								
	1978	10	17	21	56	13	33.67	57.04	8.2								
	1978	10	19	6	12	48	33.41	56.97	11.84								
4							33.68	57.04	11.61	135	0	90	90	315	90	0	225
	1978	10	15	7	29	56	33.67	57.06	11.31								
	1978	10	16	23	54	57	33.68	57.02	11.91								
5							33.67	57.06	7.92	156	30	30	60	344	60	60	246
	1978	10	10	20	15	38	33.54	57.05	9.11								
	1978	10	19	6	17	24	33.69	57.03	6.07								
	1978	10	19	23	42	46	33.67	57.08	8.57								
6							33.65	57.12	9.63	147	24	21	27	297	67	64	235
	1978	10	4	14	24	46	33.67	57.09	10.71								
	1978	10	5	12	58	22	33.65	57.11	8.07								
	1978	10	6	13	33	39	33.62	57.13	9.02								
	1978	10	7	4	8	37	33.67	57.13	10.67								
	1978	10	12	7	19	5	33.64	57.13	10.45								
	1978	10	18	15	56	37	33.68	57.11	8.87								
7							33.63	57.07	10.84	156	34	32	86	356	56	54	248
	1978	10	7	19	14	31	33.63	57.04	11.21								
	1978	10	16	7	8	47	33.64	57.08	10.97								
	1978	10	16	18	53	18	33.62	57.08	10.33								
8	1978	10	8	16	44	36	33.62	57.07	10.77	132	20	20	42	312	70	70	222
9	1978	10	19	11	17	50	33.62	57.09	10.88	147	90	90	90	327	0	0	57
							33.62	57.12	11.81	152	50			302	42		
10	1978	10	15	23	34	48	33.62	57.112	11.43			45	33			39	241
	1978	10	15	23	34	48	33.62	57.118	12.19								
11							33.57	57.08	10.13	147	74	74	57	327	16	16	237
	1978	10	6	8	30	51	33.55	57.1	9.38								
	1978	10	8	8	47	7	33.55	57.08	11.69								
	1978	10	14	14	42	2	33.57	57.08	9.04								
	1978	10	16	18	12	0	33.73	57.08	10.44								
12							33.56	57.106	10.85	158	34	34	68	338	56	56	248
	1978	10	1	2	46	13	33.55	57.1	11.8								
	1978	10	6	2	25	9	33.57	57.1	8.45								
	1978	10	7	19	38	47	33.56	57.11	10.79								
	1978	10	15	6	4	51	33.57	57.1	12.39								
13							33.55	57.15	11.95	151	40	40	61	331	50	50	241
	1978	10	1	8	8	29	33.55	57.1	12.4								
	1978	10	1	10	16	41	33.54	57.12	11.51								
14							33.53	57.031	10.42	154	48	48	64	335	42	42	245
	1978	10	14	22	57	16	33.52	57.02	11.2								
	1978	10	16	3	39	44	33.32	5701	9.65								
15							33.55	57.1	10.28	146	90	90	90	326	0	0	236
	1978	10	6	6	38	26	33.57	57.8	8.19								
	1978	10	14	21	39	56	33.55	57.1	11.29								
	1978	10	18	5	21	17	33.54	57.1	12.44								
	1978	10	20	15	40	43	33.55	57.11	9.23								
16	1978	10	5	14	50	31	33.54	57.1	10.84	168	32	31	60	330	58	57	258
17	1978	10	19	14	39	56	33.52	57.11	11.91	154	36	30	28	298	60	55	243
18							33.49	57.188	10.07	162	90	90	90	342	0	0	252
	1978	10	1	5	50	29	33.27	57.19	9.81	162	90			342	0		
	1978	10	8	18	28	41	33.07	57.19	9.68								
	1978	10	20	21	38	32	33.53	57.17	10.71								
19	1978	10	15	0	30	58	33.49	57	11.98	155	90	90	90	335	0	0	252

Basement - continuation

No.	yyyy	mm	dd	hh	Mm	ss	Lat.(N)	Long.(E)	Depth	NP1		S1		NP2		S2	
									(Km)	Str	Dp	Dp	Str	Str	Dp	Dp	Str
20							33.47	57.2	11.15	137	30	26	77	347	64	60	227
	1978	10	2	7	58	7	33.47	57.21	11.38								
	1978	10	12	23	42	53	33.48	57.19	10.92								
21	1978	10	7	14	39	17	33.43	57.075	11.56	164	46	46	70	340	44	44	254
22	1978	10	13	15	3	43	33.43	57.06	11.93	154	80	30	148	238	60	10	244
23							33.42	57.1	11.43	122	50	56	48	126	42	40	212
	1978	10	2	23	8	13	33.4	57.11	12.04								
	1978	10	4	5	39	18	33.44	57.1	11.86								
	1978	10	11	21	20	16	33.42	57.11	11.41								
24							33.42	57	9.93	152	26	25	45	314	64	64	242
	1978	10	6	13	8	12	33.43	57.19	8.82								
	1978	10	16	0	37	0	33.42	57.21	11.04								
25	1978	10	9	1	42	24	33.4	57.07	11.43	144	54	48	90	358	44	38	233
26	1978	10	3	4	53	40	33.42	57.116	10.51	131	70	45	12	260	30	18	225
27							33.39	57.2	11.83	130	7	7	40	310	83	83	220
	1978	10	8	21	46	2	33.29	57.19	11.75								
	1978	10	9	20	56	11	33.4	57.22	11.91								
28	1978	10	16	21	16	56	33.4	57.26	8.27	140	22	21	56	326	68	68	230
29	1978	10	5	2	53	16	33.39	57.27	11.02	147	16	16	57	327	74	74	237
30	1978	10	13	23	4	5	33.37	57.35	11.64	179	6	6	89	359	84	84	269
31	1978	10	2	13	26	37	33.38	57.36	11.96	134	40	40	44	314	50	50	224
32							33.37	57.15	9.95	144	38	40	40	310	52	52	222
	1978	10	8	21	33	40	33.39	57.13	9.14								
	1978	10	13	18	46	18	33.36	57.16	10.76								
33							33.36	57.35	10.94	146	10	10	56	326	80	80	326
	1978	10	11	17	51	46	33.36	57.36	10.52								
	1978	10	11	21	17	58	33.36	57.35	11.09								
	1978	10	16	15	53	44	33.35	57.33	11.21								
34							33.34	57.29	9.79	127	32	30	58	328	59	59	238
	1978	10	9	13	19	34	33.33	57.28	11.58								
	1978	10	9	16	4	38	33.24	57.28	8								
35							33.18	57.32	10.23	175	18	18	85	355	72	72	265
	1978	10	3	2	46	58	33.32	57.32	10.83								
	1978	10	8	17	16	48	33.33	57.33	9.93								
	1978	10	11	7	5	0	33.32	57.33	9.94								

Sedimentary Cover

No.	yyyy	mm	dd	hh	Mm	ss	Lat.(N)	Long.(E)	Depth	NP1		S1		NP2		S2	
									(Km)	Str	Dp	Dp	Str	Str	Dp	Dp	Str
1	1978	10	13	12	5	34	33.61	57.09	12.12	151	32	22	13	283	68	58	241
2							33.6	57.091	12.98	140	0	0	50	320	90	90	90
	1978	10	6	18	14	2	33.6	57.11	13.18								
	1978	10	15	3	40	42	33.59	57.02	11.93								
	1978	10	19	5	17	19	33.61	57.06	14.38								
3							33.58	57.12	13.24	126	0	0	36	306	90	90	90
	1978	10	3	8	6	55	33.58	57.1	13.47								
	1978	10	3	9	5	39	33.57	57.15	12.14								
	1978	10	20	3	24	30	33.58	57.12	14.12								
4	1978	10	8	2	40	1	33.5	56.91	12.4	157	90	0	67	337	0	90	90
5							33.48	56.98	13.67	158	72	72	68	158	18	18	248
	1978	10	2	20	1	49	33.48	56.99	15.12								
	1978	10	7	13	15	58	33.48	56.97	12.23								
6							33.47	57.06	12.41	156	54	42	114	204	48	37	246
	1978	10	8	7	18	57	33.47	57.08	12.54								
	1978	10	17	3	12	53	33.48	57.04	12.29								
7							33.47	57.09	12.91	148	22	22	58	328	68	68	238
	1978	10	18	1	24	44	33.47	57.08	12.96								
	1978	10	18	3	29	32	33.47	57.05	12.86								
8							33.46	57.24	12.29	140	0	0	50	320	90	90	90
	1978	10	5	3	44	19	33.46	57.2	11.68								
	1978	10	7	5	53	5	33.46	57.242	12.5								
	1978	10	20	2	5	41	33.48	57.27	12.69								
9							33.46	57.2	12.5	162	8	8	72	342	82	82	252
	1978	10	6	13	14	30	33.47	57.23	12.1								
	1978	10	18	18	46	41	33.45	57.17	12.9								
10	1978	10	11	14	9	46	33.44	56.99	15.39	144	74	74	54	324	16	16	234
11	1978	10	20	13	58	29	33.43	57.14	15.89	159	52	52	69	340	28	28	250
12	1978	10	8	12	57	36	33.43	56.93	12.24	184	70	70	106	196	21	20	273
13	1978	10	6	10	34	15	33.43	56.99	16.18	120	14	14	30	300	75	75	210
14							33.43	57.22	12.87	143	12	12	43	223	78	78	233
	1978	10	1	10	49	47	33.25	57.15	12.63								
	1978	10	6	10	59	20	33.43	57.21	12.15								
	1978	10	9	23	10	17	33.45	57.19	13.83								
15	1978	10	11	8	15	20	33.42	57.04	14.59	170	82	82	80	350	8	8	260
16	1978	10	9	17	51	36	33.4	57.042	17.17	148	37	37	58	330	53	53	240
17							33.41	57.21	12.29	146	10	10	56	326	80	80	236
	1978	10	2	9	8	3	33.42	57.25	12.5								
	1978	10	19	6	44	55	33.41	57.18	13.49								
	1978	10	19	23	50	45	33.41	57.2	10.9								
18	1978	10	19	16	10	32	33.1	56.98	15.61	158	83	83	68	338	7	7	248

Sedimentary Cover – continuation

No.	yyyy	mm	dd	hh	Mm	ss	Lat.(N)	Long.(E)	Depth	NP1		S1		NP2		S2	
									(Km)	Str	Dp	Dp	Str	Str	Dp	Dp	Str
19	1978	10	14	2	43	29	33.39	57.06	14.99	145	54	54	55	325	26	26	235
20	1978	10	11	2	38	47	33.37	57.55	15.92	132	10	10	42	312	80	80	222
21	1978	10	12	15	1	38	33.35	57.35	11.31	298	20	20	208	118	70	70	28
22	1978	10	9	16	4	36	33.34	57.35	18.01	322	26	20	191	101	70	64	53
23		10	18	6	19	58	33.32	57.23	14.68	124	36	36	34	326	56	56	236
	1978						33.3	57.3	12.2	143	26			323	64		
24		10	2	16	46	41	33.3	57.31	10.7			26	53			64	233
	1978	10	8	15	58	42	33.31	57.3	13.11								
	1978	10	8	23	25	18	33.31	57.3	14.43								
	1978	10	9	18	52	12	33.29	57.28	10.59								
25	1978						33.305	57.28	12.54	151	0	0	61	331	90	90	90
8							33.46	57.24	12.29	140	0	0	50	320	90	90	90
	1978	10	5	3	44	19	33.46	57.2	11.68								
	1978	10	7	5	53	5	33.46	57.242	12.5								
	1978	10	20	2	5	41	33.48	57.27	12.69								
9							33.46	57.2	12.5	162	8	8	72	342	82	82	252
	1978	10	6	13	14	30	33.47	57.23	12.1								
	1978	10	18	18	46	41	33.45	57.17	12.9								
10	1978	10	11	14	9	46	33.44	56.99	15.39	144	74	74	54	324	16	16	234
11	1978	10	20	13	58	29	33.43	57.14	15.89	159	52	52	69	340	28	28	250
12	1978	10	8	12	57	36	33.43	56.93	12.24	184	70	70	106	196	21	20	273
13	1978	10	6	10	34	15	33.43	56.99	16.18	120	14	14	30	300	75	75	210
14							33.43	57.22	12.87	143	12	12	43	223	78	78	233
	1978	10	1	10	49	47	33.25	57.15	12.63								
	1978	10	6	10	59	20	33.43	57.21	12.15								
	1978	10	9	23	10	17	33.45	57.19	13.83								
15	1978	10	11	8	15	20	33.42	57.04	14.59	170	82	82	80	350	8	8	260
16	1978	10	9	17	51	36	33.4	57.042	17.17	148	37	37	58	330	53	53	240
17							33.41	57.21	12.29	146	10	10	56	326	80	80	236
	1978	10	2	9	8	3	33.42	57.25	12.5								
	1978	10	19	6	44	55	33.41	57.18	13.49								
	1978	10	19	23	50	45	33.41	57.2	10.9								
18	1978	10	19	16	10	32	33.1	56.98	15.61	158	83	83	68	338	7	7	248
19	1978	10	14	2	43	29	33.39	57.06	14.99	145	54	54	55	325	26	26	235
20	1978	10	11	2	38	47	33.37	57.55	15.92	132	10	10	42	312	80	80	222
21	1978	10	12	15	1	38	33.35	57.35	11.31	298	20	20	208	118	70	70	28
22	1978	10	9	16	4	36	33.34	57.35	18.01	322	26	20	191	101	70	64	53
23		10	18	6	19	58	33.32	57.23	14.68	124	36	36	34	326	56	56	236
	1978						33.3	57.3	12.2	143	26			323	64		
24		10	2	16	46	41	33.3	57.31	10.7			26	53			64	233
	1978	10	8	15	58	42	33.31	57.3	13.11								
	1978	10	8	23	25	18	33.31	57.3	14.43								
	1978	10	9	18	52	12	33.29	57.28	10.59								
25	1978						33.305	57.28	12.54	151	0	0	61	331	90	90	90